

1 **New insight into the spatiotemporal variability and source apportionments of**
2 **C₁-C₄ alkyl nitrates in Hong Kong**

3 Z.H. Ling^{1,2}, H. Guo^{2*}, I.J. Simpson³, S.M. Saunders⁴, S.H.M. Lam^{4,5}, X.P. Lyu², D.R.
4 Blake³

5 ¹ School of Atmospheric Sciences, Sun Yat-sen University, Guangzhou, China

6 ² Air Quality Studies, Department of Civil and Environmental Engineering, The Hong
7 Kong Polytechnic University, Hong Kong

8 ³ Department of Chemistry, University of California at Irvine, California, USA

9 ⁴ School of Chemistry and Biochemistry, University of Western Australia, Perth,
10 Western Australia, Australia

11 ⁵ Pacific Environment Limited, Perth, Western Australia, Australia

12

13 * Corresponding author. Tel: +852 34003962. Fax: +852 23346389. Email:
14 ceguohai@polyu.edu.hk

15

1 **Abstract**

2 C₁-C₄ alkyl nitrates (RONO₂) were measured concurrently at a mountain site, Mt.
3 Tai Mo Shan (TMS), and an urban site, Tsuen Wan (TW) at the base of the same
4 mountain in Hong Kong from September to November 2010. Although the levels of
5 parent hydrocarbons were much lower at TMS ($p < 0.05$), similar alkyl nitrate levels
6 were found at both sites regardless of the elevation difference, suggesting various
7 source contributions of alkyl nitrates at the two sites. Prior to using a positive matrix
8 factorization (PMF) model, the data at TW were divided into “meso” and “non-meso”
9 scenarios for the investigation of source apportionments with the influence of
10 mesoscale circulation and regional transport, respectively. Secondary formation was
11 the prominent contributor of alkyl nitrates in the “meso” scenario ($60 \pm 2\%$, $60.2 \pm$
12 1.2 pptv), followed by biomass burning and oceanic emissions, while biomass burning
13 and secondary formation made comparable contributions to alkyl nitrates in the
14 “non-meso” scenario, highlighting the strong emissions of biomass burning in the
15 inland Pearl River Delta (PRD) region. In contrast to TW, the alkyl nitrate levels
16 measured at TMS mainly resulted from the photo-oxidation of the parent
17 hydrocarbons at TW during mesoscale circulation, *i.e.*, valley breezes, corresponding
18 to 52-86% of the alkyl nitrate levels at TMS. Furthermore, regional transport from the
19 inland PRD region made significant contributions to the levels of alkyl nitrates
20 (~58-82%) at TMS in the “non-meso” scenario, resulting in similar levels of alkyl
21 nitrates observed at the two sites. The simulation of secondary formation pathways
22 using a photochemical box model found that the reaction of alkyl peroxy radicals
23 (RO₂) with nitric oxide (NO) dominated the formation of RONO₂ at both sites, and the
24 formation of alkyl nitrates contributed negatively to O₃ production, with average
25 reduction rates of 4.1 and 4.7 pptv/pptv at TMS and TW, respectively.

26

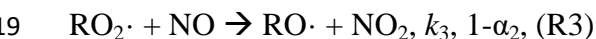
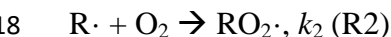
27 **Key word:** Alkyl nitrates; Source apportionment; Secondary formation; Biomass
28 burning

29

1 **1. Introduction**

2 Alkyl nitrates (RONO₂) are important photochemical pollutants in the
3 atmosphere because of their roles in local, regional and global atmospheric chemistry
4 (Jenkin et al., 2000; Seinfeld and Pandis, 2006). Alkyl nitrates are reactive nitrogen
5 compounds (NO_y) and act as a critical reservoir of nitrogen oxides (NO_x = NO + NO₂)
6 during long-range transport resulting from their relatively low reactivity (Atkinson,
7 2006).

8 A number of studies conducted in different environments have shown that alkyl
9 nitrates are either emitted from marine sources directly and/or produced indirectly
10 through photochemical reactions (Roberts et al., 1998; Blake et al., 2003; Simpson et
11 al., 2002, 2003, 2006; Reeves et al., 2007; Wang et al., 2013). In the case of biomass
12 burning, secondary alkyl nitrate formation is believed to occur by the photo-oxidation
13 of emitted hydrocarbons with a formation mechanism of RO and NO₂ (Simpson et al.,
14 2002). The photochemical pathways for the secondary formation of alkyl nitrates are
15 expressed as follows (Atkinson et al., 2006; Jenkin et al., 2000; Arey et al., 2001;
16 Sommariva et al., 2008):

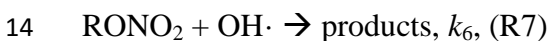


22 where k_1, k_2, k_3, k_4 and k_5 are reaction rate constants. α_1 and α_2 are branching
23 ratios for the corresponding radicals, which increase as the carbon number increases
24 and are dependent on the carbon chain length.

25 Photochemical formation of alkyl nitrates influences the oxidation of NO to NO₂,
26 subsequently leading to O₃ production by NO₂ photolysis. Therefore, alkyl nitrates are
27 often used as indicators of photochemical O₃ production (Simpson et al., 2006).
28 Furthermore, the interactions of alkyl nitrates with their parent hydrocarbons provide
29 useful information about the photochemical processing of air masses. Comparing
30 measured and predicted RONO₂/RH ratios calculated using the laboratory kinetic data

1 as a function of time, Bertman et al. (1995) examined the photochemical evolution of
2 alkyl nitrates at Scotia, Pennsylvania and the Kinterbish Wildlife Area, Alabama.
3 Since then, this approach has been used to investigate the evolution of alkyl nitrates
4 with air mass age in different regions (Simpson et al., 2006; Reeves et al., 2007;
5 Russo et al., 2010; Worton et al., 2010; Wang et al., 2013). Fairly good agreement
6 (>0.5) between measured and modeled ratios suggests that the oxidation of
7 single-parent hydrocarbons represents the evolution of their daughter alkyl nitrates,
8 while poor correlation indicated sources other than photochemical formation of alkyl
9 nitrates.

10 In contrast, the main sinks for ambient alkyl nitrates are photolysis and reactions
11 with hydroxyl radical (OH), making alkyl nitrate lifetimes vary with season, latitude
12 and altitude (days to weeks):



15 where $h\nu$ is sunlight and J_{RONO_2} and k_6 are the photolysis and OH reaction rate
16 constants, respectively. The importance of alkyl nitrate removal by photolysis
17 decreases as the carbon number increases (Clemitshaw et al., 1997; Talukdar et al.,
18 1997). Dry deposition has recently been recognized as another pathway for the
19 removal of atmospheric alkyl nitrates (Russo et al., 2010; Wu et al., 2011).

20 Despite increased concern over photochemical pollution in Hong Kong and the
21 greater Pearl River Delta (PRD) region, limited studies have focused on the
22 characteristics of alkyl nitrates, which share a common mechanism with
23 photochemical O_3 formation and act as indicators of photochemical processing. For
24 example, based on measurements conducted in 2001-2002, including during ozone
25 episodes, Simpson et al. (2006) analyzed the general characteristics of alkyl nitrates at
26 a coastal site (Tai O) in Hong Kong. C_3 - C_4 alkyl nitrates were the most abundant
27 species, with maximum and minimum levels in winter and summer, respectively. The
28 diurnal variations suggested that photochemical production was the dominant source
29 of alkyl nitrates at Tai O. Furthermore, through approximate calculations, it was
30 concluded that the methoxy radical ($\text{CH}_3\text{O}\cdot$) reaction with NO_2 was a viable

1 alternative pathway for the observed high levels of MeONO₂ during pollution
2 episodes. This mechanism was subsequently verified by Archibald et al. (2007) via
3 box model simulations, whereby RO + NO₂ → RONO₂ became important for
4 MeONO₂ formation at 10 ppb NO₂ and dominant at 35 ppb NO₂. However,
5 knowledge related to the chemical evolution and source apportionments of individual
6 alkyl nitrates and their relationship with parent hydrocarbons is still lacking in Hong
7 Kong, especially given that levels of alkyl nitrate precursors have varied since 2002
8 (Ling and Guo 2014). Hence, in this study, intensive field measurements of C₁-C₄
9 alkyl nitrates were conducted at two sites - a mountain site (Mt. Tai Mo Shan, TMS)
10 and an urban site (Tsuen Wan, TW) at the base of the same mountain in Hong Kong.
11 The data were analyzed and compared with the previous study conducted at Tai O
12 (Simpson et al., 2006). The aims were to investigate the spatiotemporal variations and,
13 for the first time, source apportionments and photochemical formation pathways and
14 evolution of alkyl nitrates in Hong Kong.

15

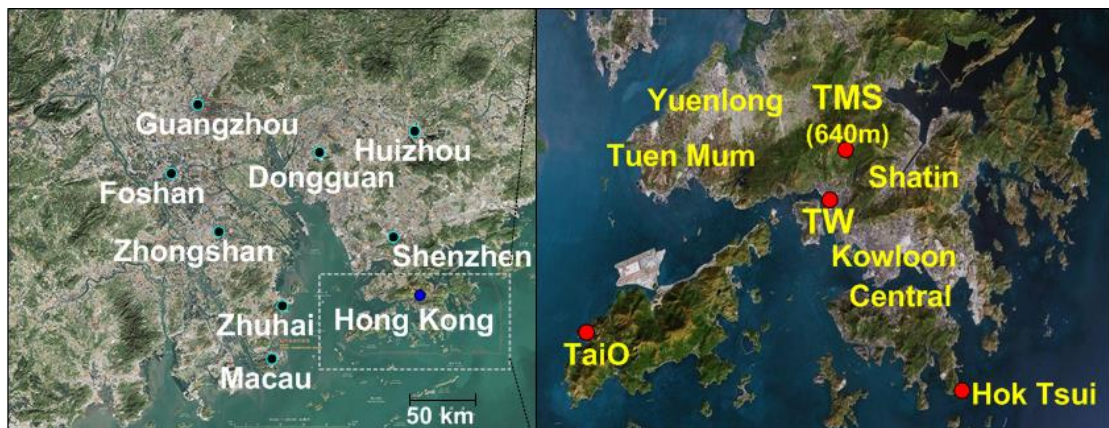
16 **2. Methodology**

17 **2.1. Sampling sites**

18 In this study, concurrent field measurements were conducted at two sites located
19 at different elevations of the highest mountain, Mt. Tai Mo Shan (TMS) with an
20 elevation of 957 m a.s.l. in Hong Kong from September 6 to November 29, 2010. A
21 detailed description of the topography of Mt. TMS was provided in an overview paper
22 (Guo et al., 2013a). In brief, Figure 1 presents the two sampling locations and the
23 surroundings. The high-elevation site (TMS) was set on the rooftop of a building on
24 the mountainside (640 m a.s.l.), the highest logistically feasible observation location,
25 beyond which the area comprised the natural landscape with shrubs and grasses to the
26 mountain summit (AFCD, 2008). The measurement site at the base of the mountain
27 was the monitoring station of the Hong Kong Environmental Protection Department
28 (HKEPD) at Tsuen Wan (TW), a mixed residential, commercial and light industrial
29 area in the New Territories of Hong Kong. The TW monitoring site was located on the
30 rooftop of a building, approximately 20 m above ground level. The linear distance

1 between the TMS and TW sites was about 7 km and the difference in elevation
2 between the two sites was 630 m. In general, the solar radiation was comparable at the
3 two sites, while the temperature was higher and the relative humidity and wind speed
4 were lower at the TW site (Guo et al., 2013a). The winds at TMS were generally from
5 the north with speeds ranging from 0.02 to 4 m s⁻¹, and the winds at TW were
6 predominantly from the southeast at speeds of 1-3 m s⁻¹ with easterly winds at night
7 and southerly winds during the day. Because of its unique topography, the air at TMS
8 was often influenced by the mountain-valley breezes and regional transport (Guo et
9 al., 2013a). Based on the average wind speed of 1.9 m/s, air masses transported from
10 upwind locations, on both local (~7 km) and regional scales (~20 km), took
11 approximately 1-3 hours to arrive at the TMS site (Guo et al., 2012, 2013a).

12 The Tai O sampling station was a rural/coastal site located on the western coast
13 of Lantau Island in southwestern Hong Kong (elevation, 80 m a.s.l.) (Figure 1). This
14 site overlooks the Pearl River Estuary to the west and north, and the South China Sea
15 to the south. It is 32 km away from the urban center to the east and about the same
16 distance from Macau/Zhuhai to the west. Major man-made sources in the region are
17 located to the east, north and southwest. Local emissions are small because of a sparse
18 population and light traffic. Owing to Asian Monsoon circulation, this site is
19 frequently affected by polluted continental air masses from the highly industrialized
20 PRD region of mainland China in cold seasons. A detailed description of the site is
21 provided in Wang et al. (2003).



22
23 Figure 1. Tai Mo Shan (TMS) and Tsuen Wan (TW) sampling sites and the
24 surrounding environments in Hong Kong.

2.2. Sampling and analysis of volatile organic compounds (VOCs)

Whole air samples were collected on 10 O₃ episode days and 10 non-O₃ episode days using evacuated 2-L stainless steel canisters. Each of the collected canister samples was integrated over a 60-min sampling period. A total of 384 samples were collected at the two sites. The O₃ episode days were selected as the days with the highest daytime hourly O₃ level at a regional scale (higher than 100 ppbv), which were based on weather forecasts and meteorological data analysis, and confirmed by the observed O₃ mixing ratios. During non-O₃ episode days, one-hour integrated samples were collected at 2-h intervals from 0700 to 1900 local time (LT) (7 samples per day). On O₃ episode days, one-hour integrated samples were collected from 0900 to 1600 LT at 1-h intervals with additional integrated samples collected at 1800, 2100, 0000, 0300 and 0700 LT (a total of 13 samples per day). After the campaign, the canister samples were sent to the University of California, Irvine (UCI) for chemical analysis. Other studies have provided detailed descriptions of the analytical system and the quality control, detection limits and analysis precision of the VOC samples (Simpson et al., 2006, 2010). In brief, the precision and detection limit of the alkyl nitrate measurements is 5% and 0.02 pptv, respectively. The calibration scale for the alkyl nitrate measurements changed in 2008, increasing by factors of 2.13, 1.81, 1.24 and 1.17 for the C₁, C₂, C₃ and C₄ alkyl nitrates, respectively (Simpson et al., 2011). In other words, the alkyl nitrates reported at Tai O by Simpson et al. (2006) were lower than the data reported here, and the Tai O data have been adjusted to the new calibration scale to allow direct comparison with this work. The Tai O sampling campaign was conducted from 24 August 2001 to 31 December 2002. Different from the air samples collected at TMS and TW, each whole-air sample at Tai O was collected for only 1-min, and was then analyzed at UCI. Intensive sampling from 0700-1900 LT was conducted every 2-h during the selected pollution episodes (17-19 October 2001, 29-30 August, 5-6 September, 9-11 and 25 October, 6-8 and 12 November 2002). Apart from the intensive sampling days, samples were taken either daily or every few days, typically in the midafternoon (Simpson et al., 2006).

1 **2.3. Continuous measurements of O₃, carbon monoxide (CO) and nitric oxide –**
2 **nitrogen dioxide – nitrogen oxides (NO-NO₂-NO_x)**

3 At TMS, online measurements of O₃, CO and NO-NO₂-NO_x were made using
4 commercial analyzers. Ozone was measured using a commercial UV photometric
5 instrument (Advanced Pollution Instrumentation (API), model 400E) that has a
6 detection limit of 0.6 ppbv. Carbon monoxide was measured with a gas filter
7 correlation, nondispersive infrared analyzer (API, Model 300E) with a heated
8 catalytic scrubber (as purchased) to convert CO to carbon dioxide (CO₂) for
9 background determination. The detection limit was 30 ppbv for a 2-min average. The
10 2σ precision was about 1% for a level of 500 ppbv (2-min average) and the overall
11 uncertainty was estimated to be 10%. NO, NO₂ and NO_x were detected with a
12 chemiluminescence NO-NO₂-NO_x analyzer (API, Model 200E) that had a detection
13 limit of 0.5 ppbv. The O₃ analyzer was calibrated weekly by using a transfer standard
14 (Thermo Environmental Instruments (TEI) 49 PS), while the other analyzers were
15 zeroed daily by analyzing scrubbed ambient air and calibrated weekly by a span gas
16 mixture with a NIST (National Institute of Standards and Technology) traceable
17 standard which was diluted to representative mixing ratios using a dynamic calibrator
18 (EnviroNics, Inc., Model 6100). The Standard (Scott-Marrin, Inc.) contained 156.5
19 ppmv CO (±2%), 15.64 ppmv SO₂ (±2%), and 15.55 ppmv NO (±2%). For the O₃,
20 CO, NO and NO_x analyzers, a data logger (Environmental Systems Corporation
21 Model 8816) was used to control the calibrations and to collect 1-minute data.

22 In addition to the above chemical measurements, several meteorological
23 parameters, including wind speed and direction, temperature, relative humidity and
24 solar radiation, were measured by the integrated sensor suite (Vantage Pro TM &
25 Vantage Pro 2 Plus TM Weather Stations, Davis Instruments).

26 At TW, hourly O₃, CO, NO-NO₂-NO_x and meteorological data were obtained
27 from the HKEPD (<http://epic.epd.gov.hk/ca/uid/airdata>). The hourly data were derived
28 by averaging 1-min data subsequently over the same time interval as the TMS data.
29 Detailed information about the measurements, quality assurance and control protocols
30 can be found in the HKEPD report (HKEPD, 2012). In addition, Table S1 in the

1 supplementary information shows descriptive statistics of main non-methane
2 hydrocarbons (NMHCs) and trace gases at both sites, while Figure S1 presents the
3 time series of trace gases and meteorological parameters at the two sites.

4 **2.4. Positive Matrix Factorization (PMF) model**

5 In this study, the US EPA PMF 3.0
6 (<http://www.epa/heads/products/pmf/pmf.html>) was used for the source
7 apportionments of the observed alkyl nitrates at TW. Our previous studies provided
8 detailed information about the PMF model (Ling et al., 2011; Ling and Guo, 2014). In
9 terms of the PMF input, the uncertainty for each species was determined as the sum of
10 10% of the VOC concentration and two times the method detection limit (MDL) of
11 the species (Paatero, 2000). Tracers for different sources were selected for the model
12 input. For example, CO, ethane and ethyne were the tracers of combustion processes,
13 and CH₃Cl was specifically used for biomass burning. DMS was a typical tracer for
14 marine emissions, while O_x (*i.e.*, O₃ + NO₂) was used as the tracer of secondary
15 formation through photochemical reactions, including the formation of alkyl nitrates,
16 because O₃ shares a common photochemical source with alkyl nitrates (Simpson et al.,
17 2006). In addition to the aforementioned species, alkyl nitrate precursors, including
18 methane, ethane, propane and *i/n*-butanes, were input into the model. In total, sixteen
19 compounds were used for the model input.

20 Various checks and sensitivity tests were conducted to examine the model
21 performance. Firstly, many different starting seeds were tested and no multiple
22 solutions were found. Secondly, the correlation between the predicted and measured
23 concentration of each species was fairly good at TW ($R^2=0.64\sim 0.94$) after the PMF
24 implementation. Thirdly, the scale residuals, which are the uncertainty over the
25 different runs for the input species, ranged between -3 and 3 for the PMF solution.
26 Fourthly, the ratios of Q(robust)/Q(true) were close to 1 for 4-factor solution, within
27 the ranges of 0.97-0.98 at TW, higher than those of 3-factor and 5-factor solutions,
28 indicating all data points were fit better in the 4-factor solution. Indeed, the extracted
29 source profiles from the 4-factor solution were the most reasonable. All the factors
30 were mapped to a base factor in all the 100 runs in the bootstrapped simulation for the

1 four-factor solution, suggesting the solution was stable. Lastly, the G-space plot
2 extracted from the F-peak model results did not present oblique edges, reflecting that
3 there was little rotation for the selected solution. Overall, the above features
4 demonstrated that PMF provided reasonable results for the source apportionment of
5 alkyl nitrates (Ling et al., 2011; Ling and Guo, 2014).

6 **2.5. Photochemical box model incorporating master chemical mechanism** 7 **(PBM-MCM)**

8 A photochemical box model coupled with Master Chemical Mechanism
9 (PBM-MCM) was used to simulate the in-situ formation of alkyl nitrates at TMS and
10 TW. The PBM-MCM was developed by assuming that it was a well-mixed box
11 without the treatment of vertical or horizontal dispersion, and the air pollutants in the
12 model were homogeneous. For the mechanism coupled in the model, the MCM
13 (version 3.2) used in this study is a state-of-the-art chemical mechanism, which
14 describes the degradation of 143 primary VOCs including methane and contains
15 around 16,500 reactions involving 5900 chemical species (Jenkin et al., 1997, 2003;
16 Saunders et al., 2003). The measured data, including O₃, CO, NO_x, SO₂, 54 VOCs and
17 methane, together with the actual meteorological conditions of temperature, relative
18 humidity and boundary layer in the region, were used to constrain the model. The
19 photolysis rates of different species in the model were parameterized as suggested by
20 the previous study (Pinho et al., 2009) using the photon flux determined from the
21 Tropospheric Ultraviolet and Visible Radiation (v5) model based on the actual
22 conditions, such as meteorological conditions, location and time period of the field
23 campaign in Hong Kong (Lam et al., 2013). The model output simulated in-situ
24 formation of alkyl nitrates and other secondary products as well as the full set of
25 precursors, radicals and intermediates. To provide robust results from the model
26 simulation, several measures were adopted for the model development. The detailed
27 information for the model frameworks, the model development and the evaluation for
28 the model performance has been reported in our previous studies (Lam et al., 2013;
29 Ling et al., 2014).

30

1 **3. Results and discussion**

2 **3.1 Descriptive statistics of alkyl nitrates and their parent hydrocarbons**

3 Table 1 presents the descriptive statistics of alkyl nitrates and their parent
4 hydrocarbons at TMS and TW. Figure 2 compares the levels of alkyl nitrates
5 measured at TMS and TW with those measured in different environments in previous
6 studies. In general, 2-PrONO₂ and 2-BuONO₂ were the most abundant alkyl nitrates
7 at the two sites, consistent with the results observed in different environments (Blake
8 et al., 2003; Simpson et al., 2006; Russo et al., 2010; Wang et al., 2013). The
9 relatively higher levels of 2-PrONO₂ and 2-BuONO₂ were associated with the balance
10 between increased branching ratios for photochemical alkyl nitrate formation and the
11 decreased lifetime of both parent alkanes and alkyl nitrates with increasing carbon
12 number (Arey et al., 2001; Simpson et al., 2006; Russo et al., 2010). In comparison,
13 the levels of MeONO₂, EtONO₂ and 2-PrONO₂ were slightly higher at TW than at
14 TMS ($p < 0.05$), with average values of 12.6 ± 0.5 (mean \pm 95% confidence interval),
15 13.3 ± 0.6 and 26.3 ± 1.2 pptv, respectively, at TW. The average mixing ratios of
16 1-PrONO₂ and 2-BuONO₂ were comparable at the two sites ($p > 0.05$). The results
17 were contradictory to the fact that the mixing ratios of their parent hydrocarbons at
18 TMS were much lower than at TW, highlighting the complexity of sources of alkyl
19 nitrates at both sites.

20 In comparison with other studies, the average mixing ratios of alkyl nitrates at
21 TMS were much higher than those measured in forested areas in coastal New England
22 (Russo et al., 2010) and in tropospheric air influenced by Asian outflow during the
23 airborne TRACE-P mission (Simpson et al., 2003), where the levels of parent
24 hydrocarbons were also lower. (Note that all of the UCI data shown in Figure 2 were
25 adjusted to UCI's post-2008 alkyl nitrates' calibration scale to enable direct
26 comparison (Simpson et al., 2011). However, the mean mixing ratios of C₁-C₃ alkyl
27 nitrates were slightly lower and the 2-BuONO₂ mixing ratio was higher at TMS than
28 at Tai O (Table 2), Hok Tsui and in Karachi, Pakistan (Barletta et al., 2002; the
29 Karachi data have also been adjusted to the new UCI alkyl nitrates' calibration scale).
30 The differences among TMS, Tai O and Hok Tsui might result not only from the

1 levels of their parent hydrocarbons, but also from the influence of air masses with
 2 different photochemical ages and sources (Wang et al., 2003). Furthermore, as
 3 mentioned in Section 2.2, the sampling method and sampling period at TMS were
 4 different from those at Tai O and Hok Tsui, where the sampling duration was only
 5 1-min and the sampling time varied on different sampling days. In particular, many
 6 whole air samples were collected during O₃ episodes at Tai O. These could also
 7 induce differences in observed levels among the three sites. At the urban TW site, the
 8 mean mixing ratios of alkyl nitrates were lower than those measured in urban areas in
 9 Europe (Worton et al., 2010) and China (Wang et al., 2013). Compared to the average
 10 values of alkyl nitrates at Tai O, the levels of EtONO₂, 1-PrONO₂ and 2-BuONO₂
 11 were slightly higher and the MeONO₂ and 2-PrONO₂ mixing ratio was lower at TW.

12

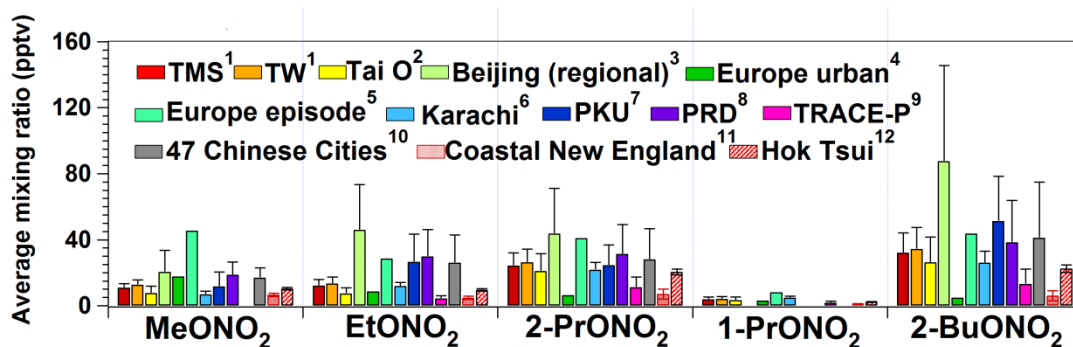
13 Table 1 Descriptive statistics of alkyl nitrates and parent hydrocarbons (pptv) in whole
 14 air samples collected at TMS and TW during the sampling period.

Species	TMS					TW				
	Mean*	Min.	Max.	10 th #	90 th #	Mean	Min.	Max.	10 th #	90 th #
MeONO ₂	10.9±0.4	6.2	21.4	8.1	13.6	12.6±0.5	7.2	26.6	9.2	16.4
EtONO ₂	12.1±0.5	3.2	25.6	7.6	16.5	13.3±0.6	4.0	35.0	8.3	18.1
2-PrONO ₂	24.1±1.1	4.0	51.2	14.8	34.7	26.3±1.2	6.0	49.2	16.2	36.2
1-PrONO ₂	3.8±0.2	0.4	10.6	1.9	5.5	4.0±0.2	0.7	8.1	2.2	6.1
2-BuONO ₂	32.0±1.7	3.1	80.1	18.8	46.6	34.2±1.9	5.1	92.8	20.8	49.2
Methane (ppmv)	2.0±0.1	1.8	2.2	1.9	2.0	2.0±0.1	1.8	2.5	1.9	2.0
Ethane	1908±78	396	3588	1154	2470	2224±90	717	4315	1359	2906
Propane	1101±75	106	4455	569	1749	3551±415	1443	33800	1844	5153
<i>n</i> -Butane	830±91	97	6252	349	1517	4486±482	1372	34700	2168	7633

15 * Average ± 95% confidence interval

16 # 10th and 90th percentiles

17



18

1 Figure 2. Comparison of alkyl nitrate mixing ratios in different locations. Data
 2 collected by UCI before 2008 (PRD and TRACE-P) were adjusted to UCI's new
 3 calibration scale to permit direct comparison (see text for details about the new
 4 calibration.

5 ¹. This study, September-November, 2010. ². Rural site, August 2001-December 2002 (Simpson et
 6 al., 2006). ³. Urban site, 2009-2011 (Wang et al., 2013). ⁴. Urban sites, April-May 2004 (Worton et
 7 a., 2010). ⁵. Urban sites, April-May 2004 (Worton et al., 2010). ⁶. Coastal site, December
 8 1998-January1999 (Barletta et al., 2002). ⁷. Urban site, August-September 2011 and December
 9 2011-January 2012 (Wang et al., 2013). ⁸. Regional background sites, September 2009 (Wang et al.,
 10 2013). ⁹. Aircraft measurement, February-April 2001 (Simpson et al., 2003). ¹⁰. Urban sites, July
 11 2009 (Wang et al., 2013). ¹¹. Coastal site, January-February and June-August 2002, July-August
 12 2004 (Russo et al., 2010). ¹². Regional background site, March 2001-April 2002 (unpublished
 13 data).

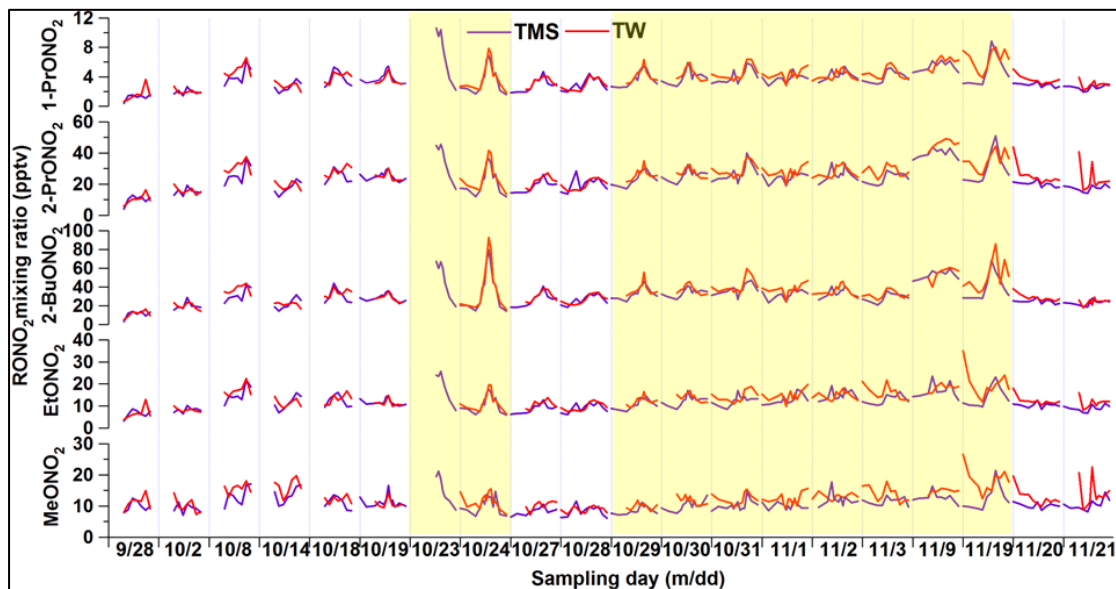
14
 15
 16 Table 2 Descriptive statistics of alkyl nitrate (pptv) and parent hydrocarbons (ppbv) in
 17 whole air samples collected at Tai O between 24 August 2001 and 31 December 2002
 18 (from Simpson et al., 2006).

Compound	Minimum	Maximum	Median	Mean
MeONO ₂	5.5	52.2	13.4	15.9
EtONO ₂	2.7	34.3	12.1	13.1
1-PrONO ₂	0.2	14.5	3.5	3.9
2-PrONO ₂	2.4	65.9	24.5	32.6
2-BuONO ₂	0.8	89.8	27.4	30.7
Methane (ppmv)	1.75	3.70	1.96	2.05
Ethane (ppbv)	0.38	5.05	2.14	2.12
Propane (ppbv)	0.006	13.0	1.54	2.05
<i>n</i> -Butane (ppbv)	0.006	12.8	0.95	1.64

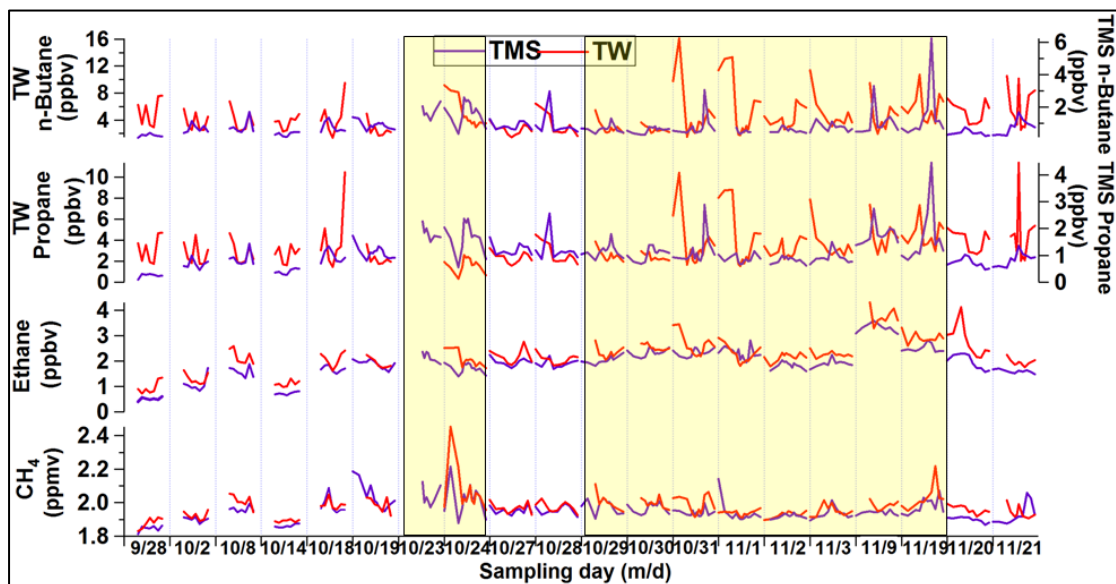
19
 20 Table S2 and Figure S2 in the supplementary information summarize the
 21 synoptic weather conditions and the corresponding variations of O₃ and alkyl nitrates
 22 on O₃ episode and non-O₃ episode days at both sites. In general, meteorological
 23 conditions including temperatures, winds and solar radiation significantly influenced
 24 the levels of air pollutants (Table S2). High mixing ratios of O₃ and alkyl nitrates were
 25 usually associated with meteorological conditions with high-pressure system and/or
 26 stable conditions, such as high temperatures, intense solar radiation and low wind
 27 speeds. Figure 3 shows the time series of C₁-C₄ alkyl nitrates on O₃ episode and
 28 non-O₃ episode days at both sites, while Figure 4 presents the temporal variations of

1 their parent hydrocarbons accordingly. Although the ranges of alkyl nitrate mixing
2 ratios were similar and maximum values were observed in the afternoon, the
3 day-to-day variations of individual alkyl nitrates differed during the sampling period
4 at both sites. The maximum values were comparable and the diurnal patterns tracked
5 each other for the C₃-C₄ alkyl nitrates at TMS and TW, especially on the days (24
6 October to 3 November, 9 and 19 November) with relatively higher O₃ mixing ratios
7 ($p < 0.05$). The average daytime O₃ mixing ratios (0700-1800) on the high O₃ days
8 were 77 ± 3 and 38 ± 3 ppbv at TMS and TW, respectively, compared to 58 ± 3 and
9 23 ± 3 ppbv, on the non-O₃ episode days. Typically, the average daytime levels of
10 2-PrONO₂, 1-PrONO₂ and 2-BuONO₂ on high O₃ days at TMS were 27 ± 1 (TW: 28
11 ± 1), 4.5 ± 0.3 (4.4 ± 0.2) and 37 ± 2 (39 ± 3) pptv, respectively, higher than those on
12 non-O₃ episode days ($p < 0.05$), implying that secondary formation of alkyl nitrates
13 might be more prominent on O₃ episode days. Coincident with the high C₃-C₄ alkyl
14 nitrates during high O₃ days, their parent hydrocarbons, *i.e.*, propane (0.56-4.46 and
15 1.55-10.4 ppbv for TMS and TW, respectively) and *n*-butane (0.28-6.25 and 1.47-16.1
16 ppbv, respectively) also showed elevated mixing ratios (Figure 4), further suggesting
17 an important source of C₃-C₄ alkyl nitrates which was photo-oxidation of the parent
18 hydrocarbons. For the C₁-C₂ alkyl nitrates, the temporal patterns of MeONO₂ and
19 EtONO₂ were different at the two sites, especially on high-level O₃ days. The peaks of
20 MeONO₂ and EtONO₂ were usually observed between 11 a.m. and 4 p.m. at TMS,
21 except for 14 and 28 October, 1-2, 9, 20-21 November. The peaks of C₁-C₂ alkyl
22 nitrates corresponded to the high levels of methane and ethane observed at 11 a.m. to
23 5 p.m., likely resulted from regional transport (Guo et al., 2009; Jiang et al., 2010)
24 and/or mesoscale circulations (Gao et al., 2005; Wang et al., 2006) (Section 3.2.3). At
25 TW, however, besides the maximum concentrations observed in the afternoon, high
26 levels of MeONO₂ and EtONO₂ were observed from midnight to early morning on 13
27 out of the 19 sampling days (*i.e.*, 2, 8, 14, 24, 28, 30-31 October, 1-3, 19-21
28 November), when the prevailing winds switched to the southeast direction, implying
29 that the high levels of MeONO₂ and EtONO₂ are likely related to marine emissions
30 and aged continental plumes which were re-circulated from the South China Sea to

1 the coastal urban site at night. Indeed, this speculation was supported by the source
 2 apportionment results at TW, which confirmed that the high MeONO₂ and EtONO₂
 3 levels from midnight to early morning on the above sampling days were related to
 4 oceanic emissions (see Section 3.2.2 for details).



5
 6 Figure 3. Time series of MeONO₂, EtONO₂, 1-PrONO₂, 2-PrONO₂ and 2-BuONO₂
 7 measured at TMS (purple) and TW (red) in 2010. The yellow shading highlights the
 8 O₃ episode days.



10
 11 Figure 4. Time series of the parent hydrocarbons of alkyl nitrates at TMS and TW.
 12 The yellow shading highlights the O₃ episode days.

13
 14 Although the levels of the parent hydrocarbons were lower at TMS, similar

1 values of alkyl nitrates were observed at both sites, regardless of the elevation,
 2 suggesting the contributions of different sources and/or the influences of different air
 3 masses. Hence, the source apportionments of alkyl nitrates, contributions of reaction
 4 pathways for the secondary formation of alkyl nitrates, and the relationship between
 5 O₃ and alkyl nitrates were analyzed in the following sections.

6 **3.2. Sources of alkyl nitrates**

7 **3.2.1. Photochemical evolution of alkyl nitrates**

8 As photochemical oxidation of parent hydrocarbons is an important source of
 9 alkyl nitrates, it is valuable to study the photochemical evolution of alkyl nitrates. To
 10 do so, the relationships of alkyl nitrates with their parent hydrocarbons at the two sites
 11 were further examined using a simplified sequential reaction model developed by
 12 Bertman et al. (1995) (Equation 1), based on the assumptions that: (i) the hydrogen
 13 abstraction reaction from the parent hydrocarbon was the rate-limiting step for
 14 photochemical production of alkyl nitrates, and (ii) the reaction environment was
 15 NO_x-rich, making the reaction with NO being the dominant pathway for the removal
 16 of RO₂ radicals (Russo et al., 2010). In this study, the average mixing ratios of NO_x at
 17 TMS and TW were 10.7 ± 0.3 and 56.3 ± 1.6 ppbv, respectively, indicating that the
 18 environment was NO_x-rich (> 0.1 ppbv, Roberts et al., 1998). Hence, reaction with
 19 NO was the main pathway for the removal of RO₂ radicals at the two sites. In addition,
 20 the results of PBM-MCM model simulation confirmed that the hydrogen abstraction
 21 reaction from the parent hydrocarbon, namely the reaction of hydrocarbon with OH
 22 radical, was indeed the rate-limiting step for photochemical production of alkyl
 23 nitrates at both sites (Lyu et al., 2015).

$$24 \quad \frac{RONO_2}{RH} = \frac{\beta k_A}{k_B - k_A} (1 - e^{(k_A - k_B)t}) + \frac{[RONO_2]_0}{[RH]_0} e^{(k_A - k_B)t} \quad (\text{Equation 1})$$

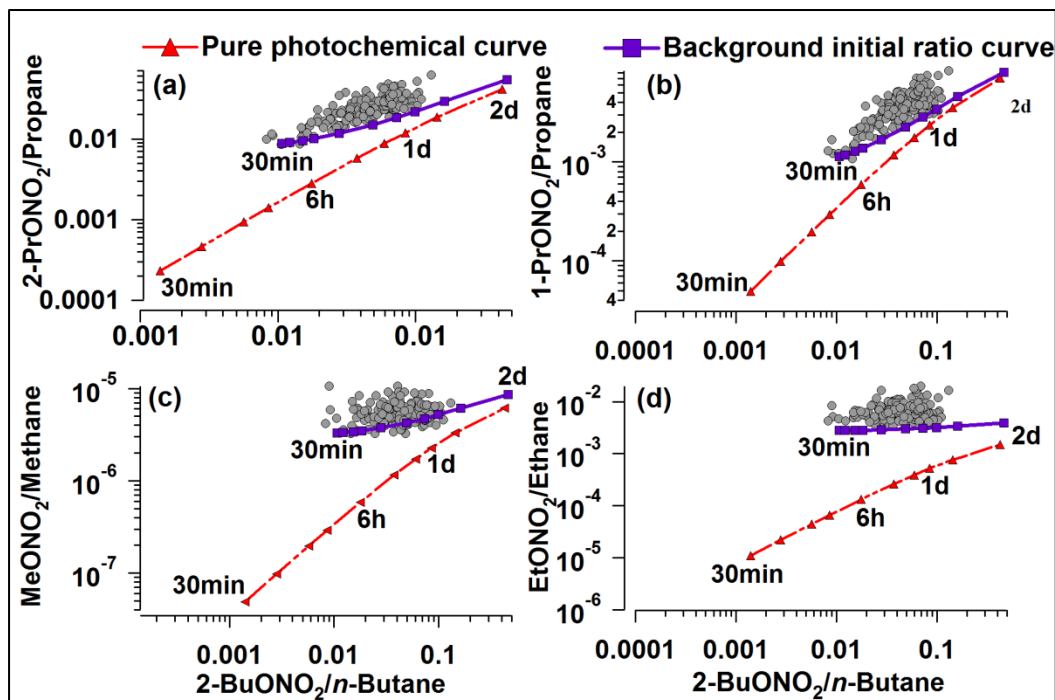
25 where $\beta = \alpha_1 \alpha_2$, k_A is the production rate for the formation of alkyl nitrates
 26 through the oxidation of hydrocarbons, RH ($k_A = k_1[\text{OH}]$), while k_B is the destruction
 27 rate for alkyl nitrates through photolysis and the reaction with OH ($k_B = k_5[\text{OH}] +$
 28 J_{RONO_2}). $[RONO_2]_0$ and $[RH]_0$ are the initial concentrations of alkyl nitrates and the
 29 parent hydrocarbons before photochemical processing, respectively; $[\text{OH}]$ is the

1 diurnal average concentration of the OH radical. The relationships of alkyl nitrates
2 with their parent hydrocarbons derived from the preceding equation are comparatively
3 independent of the variations of OH and photolysis rates of alkyl nitrates (Roberts et
4 al., 1998; Wang et al., 2013). If the initial concentrations of alkyl nitrates and RH are
5 zero, Equation 1 can be expressed as follows (Equation 2):

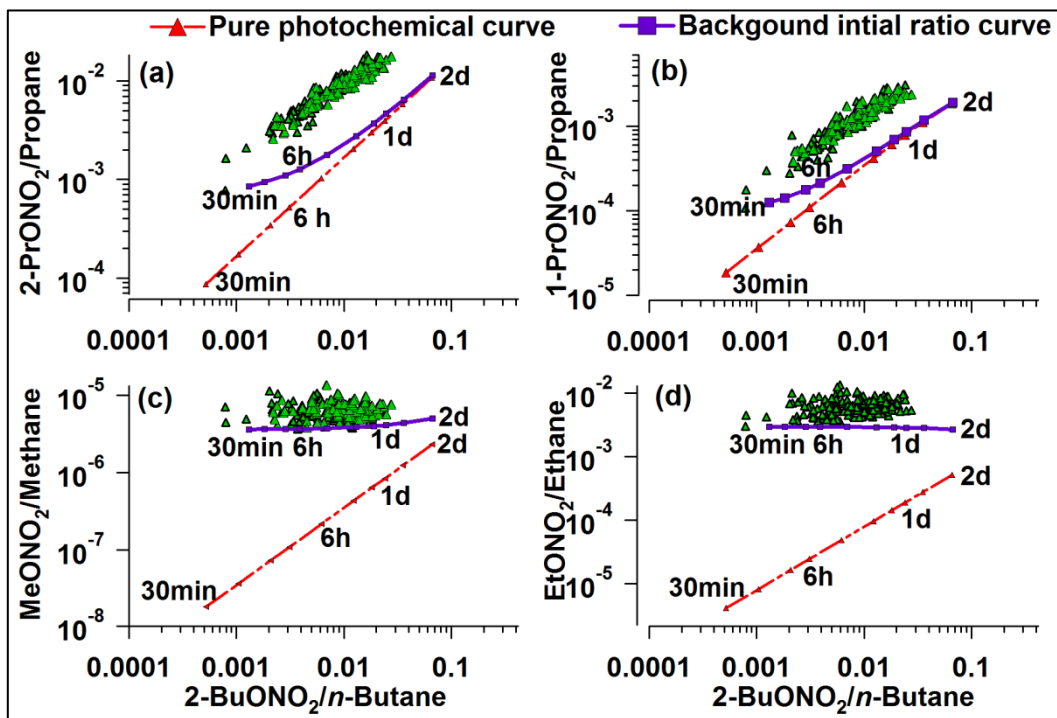
$$6 \quad \frac{RONO_2}{RH} = \frac{\beta k_A}{k_B - k_A} (1 - e^{(k_A - k_B)t}) \quad (\text{Equation 2})$$

7 The relationships between alkyl nitrates and RH are obtained by plotting the
8 measured ratios of $RONO_2/RH$ to a specific ratio, 2-BuONO₂/*n*-butane. The
9 2-BuONO₂/*n*-butane ratio has been widely used in the analysis of alkyl nitrates because
10 *n*-butane is typically one of the most abundant hydrocarbons and 2-BuONO₂ is the
11 dominant alkyl nitrate (Roberts et al., 1998; Wang et al., 2013; Worton et al., 2010).
12 Although some studies have investigated the relationships between alkyl nitrates and
13 their parent hydrocarbons using zero initial values of alkyl nitrates, more recent
14 studies have used non-zero initial values of alkyl nitrates to evaluate the influence of
15 background levels on the photochemical evolution of alkyl nitrates (Reeves et al.,
16 2007; Russo et al., 2010; Wang et al., 2013). Therefore, in addition to zero initial
17 ratios, non-zero initial ratios of $RONO_2/RH$, equal to the lowest values from 0000 to
18 0700 measured at TMS and TW, respectively, as suggested by Wang et al. (2013),
19 were used to investigate the relationships between alkyl nitrates and their parent
20 hydrocarbons in this study. The diurnal average OH mixing ratios were simulated
21 using the PBM-MCM (Lyu et al., 2016). By providing the values of photochemical
22 processing time (*t*), the predicted ratios of $RONO_2/RH$ were calculated since other
23 parameters, *i.e.*, k_A , k_B , α_1 , α_2 and J_{RONO_2} were obtained from literature (Clemitshaw et
24 al., 1997; Simpson et al., 2003; Worton et al., 2010; Wang et al., 2013). In this study,
25 the given photochemical processing time ranged from 30 min to 2 days. The curves
26 generated with zero initial values were the pure photochemical (PP) curves for the
27 evolution of alkyl nitrates, and the curves with non-zero values, defined as
28 background initial ratio (BIR) curves, were generated by assuming that both
29 photochemical formation and background levels contributed to the distribution of

1 alkyl nitrates (Russo et al., 2010; Wang et al., 2013). Consistent with previous studies
 2 (Russo et al., 2010; Wang et al., 2013), the shapes of the BIR curves were different
 3 from those of PP curves. The BIR curves of C₁-C₃ alkyl nitrates at both sites were
 4 positioned above their PP curves at shorter processing time ($t < 1$ d) and converged
 5 towards the PP curves at longer processing times ($t = 1.5$ -2 d) (Figure 5), resulting
 6 from the decreased influence of the parameter $\frac{[RONO_2]_0}{[RH]_0} e^{(k_A - k_B)t}$ on the difference
 7 between the two curves as the photochemical age increased (Wang et al., 2013). This
 8 feature was more pronounced for C₃-C₄ alkyl nitrates at TW (Figure 6) because of the
 9 lower values of $[RONO_2]_0/[RH]_0$ resulting from the high mixing ratios of propane and
 10 *n*-butane (Ling and Guo, 2014). Figure 5 presents the relationships of C₁-C₃
 11 $RONO_2/RH$ to 2-BuONO₂/*n*-butane at TMS. The red dashed curves are pure
 12 photochemical curves, while the blue solid curves are BIR curves with the lowest
 13 ratios of $RONO_2/RH$ from 0000 to 0700 LT as the background initial ratio. Similarly,
 14 Figure 6 shows the relationships of C₁-C₃ $RONO_2/RH$ to 2-BuONO₂/*n*-butane at TW.



15
 16 Figure 5. Relationships of C₁-C₃ $RONO_2/RH$ with 2-BuONO₂/*n*-butane at TMS. The
 17 red dashed curves were obtained based on zero initial concentrations of RH and alkyl
 18 nitrates (pure photochemical curves, PP), while the blue solid curves were obtained
 19 based on non-zero initial levels (background initial ratio curves, BIR), with the lowest
 20 ratios of $RONO_2/RH$ from 0000 to 0700 LT.



1

2 Figure 6. Relationships of C₁-C₃ RONO₂/RH with 2-BuONO₂/*n*-butane at TW. The
 3 red dashed curves were obtained based on zero initial concentrations of RH and alkyl
 4 nitrates (pure photochemical curves, PP), while the blue solid curves were obtained
 5 based on non-zero initial levels (background initial ratio curves, BIR), with the lowest
 6 ratios of RONO₂/RH from 0000 to 0700 LT.

7

8 At TMS, the measured ratios of MeONO₂/methane and EtONO₂/ethane to
 9 2-BuONO₂/*n*-butane were much higher than the ratios in the PP curves (Figure 5c &
 10 d), with the observed ratios larger than their theoretical ratios by factors of 5-25. As
 11 expected, the observed trends approached the PP curves at a longer processing time,
 12 suggesting that the measured ratios of C₁-C₂ RONO₂/RH to 2-BuONO₂/*n*-butane were
 13 influenced by aged air masses resulting from their relatively long atmospheric
 14 lifetimes and the slow photochemical reaction rates of methane and ethane (Worton et
 15 al., 2010; Russo et al., 2010). However, the difference between the measured ratios
 16 and the predicted ratios of C₁-C₂ RONO₂/RH to 2-BuONO₂/*n*-butane in BIR curves
 17 was comparatively smaller, further confirming that there were other sources
 18 contributing to ambient C₁-C₂ alkyl nitrates besides photochemical formation,
 19 including the background levels of C₁-C₂ alkyl nitrates and their parent hydrocarbons
 20 (direct measurements of RH in Table 1) (Wang et al., 2013). For example, the average

1 MeONO₂ and EtONO₂ mixing ratios at Hok Tsui, a PRD regional background site,
2 were 10.4 ± 0.7 and 9.6 ± 0.7 pptv (unpublished data, 2001-2002), respectively.

3 Regarding the C₃ alkyl nitrates, the measured ratios of 1- and 2-PrONO₂/propane
4 to 2-BuONO₂/*n*-butane were closer to the ratios of the BIR curve than those of the PP
5 curve at TMS, further indicating the influence of background C₃ alkyl nitrates and
6 their parent hydrocarbons. However, the evolution of the measured ratios of C₃
7 RONO₂/RH to 2-BuONO₂/*n*-butane agreed well with the predicted ratios of BIR and PP
8 curves at TMS, indicating that secondary formation from propane oxidation
9 contributed significantly to the ambient C₃ alkyl nitrates, including the background C₃
10 alkyl nitrates. Consistent with previous studies, the slopes of the observed ratios of C₃
11 RONO₂/RH to 2-BuONO₂/*n*-butane were different from those in the PP and BIR
12 curves (Russo et al., 2010; Wang et al., 2013). For example, the slopes of the observed
13 ratios of 1- and 2-PrONO₂/propane to 2-BuONO₂/*n*-butane were 0.04 ± 0.01 and 0.26
14 ± 0.02 , respectively, while the slopes for the BIR curves were 0.02 ± 0.01 (PP curve:
15 0.02 ± 0.01) and 0.12 ± 0.01 (0.10 ± 0.01), respectively. This was reasonable as the
16 difference in the number of samples and distribution of data between the observed
17 ratios and the ratios of PP and BIR curves, particularly when the observed ratios were
18 higher than the theoretical ones because of significant influence of the background
19 levels of alkyl nitrates and RH (Russo et al., 2010; Wang et al., 2013). Therefore, to
20 further investigate the influence of secondary formation and background mixing ratios
21 on C₃ alkyl nitrates at TMS, the ratio of 1-/2-PrONO₂ was examined. Previous studies
22 reported that the theoretical ratio of 1-/2-PrONO₂ was the ratio between the yield for
23 1-PrONO₂ and 2-PrONO₂ formation, which was equal to the ratio of
24 $\beta_{1\text{-PrONO}_2}/\beta_{2\text{-PrONO}_2}$ (0.21) (Simpson et al., 2003; Wang et al., 2013). If photochemical
25 production was the dominant source of 1-PrONO₂ and 2-PrONO₂, the observed ratios
26 should be close to the theoretical ones. Indeed, the slope of 1-PrONO₂ and 2-PrONO₂
27 at TMS was 0.19 ($R^2 = 0.86$, $p < 0.05$), close to the theoretical ratio (0.21), confirming
28 that photochemical production from propane, including in-situ photochemical
29 production and transport of photochemically-formed C₃ alkyl nitrates in urban areas
30 and/or during transit from urban areas to TMS, was the dominant source of ambient

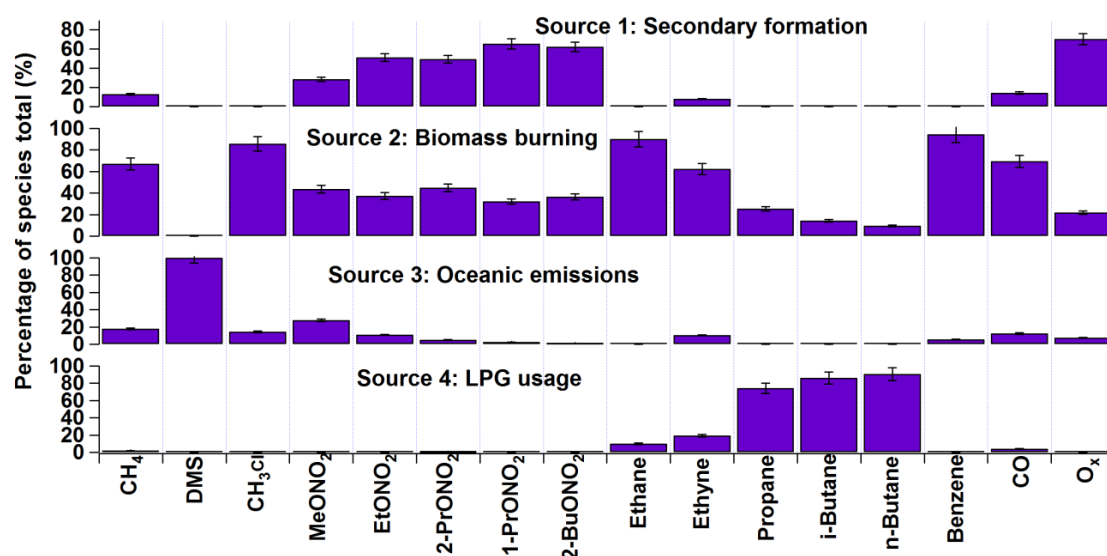
1 C₃ alkyl nitrates.

2 At TW, the comparison between the observed ratios of C₁-C₂ RONO₂/RH to
3 2-BuONO₂/*n*-butane and the ratios from the PP and BIR curves was consistent with
4 that at TMS. However, in terms of C₃ alkyl nitrates, although the evolution of the
5 measured ratios of C₃ RONO₂/RH to 2-BuONO₂/*n*-butane followed the trends of the
6 ratios in the PP and BIR curves, the measured ratios of C₃ RONO₂/RH to
7 2-BuONO₂/*n*-butane at TW were further away from the PP/BIR curves, about 2-3
8 times the ratios in the PP and BIR curves, implying additional sources of C₃ alkyl
9 nitrates (Wang et al., 2013) (details in Section 3.2.2). High emissions of propane
10 provided sufficient precursors of C₃ alkyl nitrates, and the lifetimes of 1-PrONO₂ and
11 2-PrONO₂ were long enough to sustain relatively high levels at TW. To further
12 investigate the influence of additional sources on the distributions of C₃ alkyl nitrates
13 at TW, equation 1 was used to fit the measured ratios of 1- and 2-PrONO₂/propane to
14 calculate the yield of C₃ alkyl nitrates (β). The average yields of 1- and 2-PrONO₂
15 were 0.032 ± 0.004 and 0.22 ± 0.02 , respectively, higher than the laboratory kinetic
16 values by factors of 4–9 (Kwok and Atkinson, 1995). This confirms the presence of
17 additional emissions of C₃ alkyl nitrates at TW, including locally-emitted C₃ alkyl
18 nitrates and/or secondary formation other than the production pathway from propane
19 to proxyl radical and PrONO₂ (Reeves et al., 2007; Worton et al., 2010). The slope of
20 1-PrONO₂ to 2-PrONO₂ at TW was 0.15 ($R^2 = 0.80$, $p < 0.05$), lower than the
21 theoretical ratio of 0.21, further demonstrating the influence of other significant
22 sources on ambient mixing ratios of C₃ alkyl nitrates at TW.

23 **3.2.2. Source apportionment of alkyl nitrates**

24 Figure 7 presents the explained variations of species (as a percentage of the
25 species total) in the identified sources extracted by the PMF model. The standard error
26 in Figure 7 was obtained from a bootstrap analysis of the PMF model simulation. The
27 source profiles of the alkyl nitrates and their parent hydrocarbons were altered
28 resulting from photochemical transformation during transport to the TMS site.
29 Therefore, only the data collected at the urban site were used for source
30 apportionments of alkyl nitrates.

1 High concentrations of O_x and alkyl nitrates were found in the first factor at both
 2 sites, implying that this factor was associated with secondary formation. In addition,
 3 certain amounts of combustion species, such as ethane, ethyne, propane, *i/n*-butanes,
 4 benzene and CO were present in this factor. It is not surprising that O_x correlated with
 5 the aforementioned species given that O₃ is a secondary pollutant formed from
 6 photochemical oxidation of RH (Ling and Guo, 2014). The second factor was
 7 distinguished by a significant presence of methyl chloride, ethene, ethyne and
 8 benzene along with certain amounts of methane, propane and *i/n*-butane. It is well
 9 established that methyl chloride, ethyne and benzene are typical tracers for biomass
 10 burning/biofuel combustion (Barletta et al., 2009; Guo et al., 2011). As biofuel was
 11 not in widespread use in Hong Kong (HKCSD, 2010), this factor was identified as
 12 biomass burning. The third factor was identified as oceanic emissions, as the tracer
 13 DMS had an exclusively high percentage in this source at both sites (Blake et al.,
 14 2003; Marandino et al., 2013). The last factor was dominated by high percentages of
 15 propane and *i/n*-butanes, typical tracers of liquefied petroleum gas (LPG). Therefore,
 16 this factor was identified as LPG usage.



17
 18 Figure 7. Explained variations of species in the identified sources extracted by the
 19 PMF model for TW.

20
 21 As mentioned earlier, regional transport and mesoscale circulation had a
 22 significant influence on the distribution of air pollutants at TMS and TW (Guo et al.,

1 2012, 2013a). By using the Weather Research and Forecasting (WRF) model, air
2 masses affected by mesoscale circulation were distinguished from those affected by
3 regional transport (Guo et al., 2013a). Nine sampling days during the entire sampling
4 period (24, 29-31 October, 1-3, 9 and 19 November) were identified to be affected by
5 mountain-valley breezes (they were also O₃ episode days). Hence, we divided the
6 sampling period into two categories - “meso” and “non-meso” scenarios for source
7 apportionment analysis. The “meso” scenario included the nine O₃ episode days with
8 apparent mesoscale circulation, while the “non-meso” scenario covered the rest of the
9 sampling days.

10 By summing up the mass of the alkyl nitrates in each source category, the overall
11 mixing ratios in each source were obtained and the contribution of each individual
12 source to alkyl nitrates at both sites was calculated. Figures 8 and 9 present the source
13 contributions to individual alkyl nitrates for the “meso” and “non-meso” scenarios in
14 percentage and in mixing ratio at TW, respectively. The mixing ratios of total alkyl
15 nitrates (*i.e.*, $\sum \text{RONO}_2 = \text{MeONO}_2 + \text{EtONO}_2 + 1\text{-PrONO}_2 + 2\text{-PrONO}_2 +$
16 2-BuONO_2) were higher in the “meso” scenario than those in “non-meso” scenario (p
17 < 0.05), with the average value of 100.9 ± 7.5 pptv for total alkyl nitrates in the “meso”
18 scenario, about 1.4 times those in the “non-meso” scenario. It was found that in the
19 “meso” scenario, secondary formation was the most significant contributor to the total
20 alkyl nitrate mixing ratios, with an average percentage of $60 \pm 2\%$ or absolute mixing
21 ratio of 60.2 ± 1.2 pptv, followed by biomass burning ($34 \pm 1\%$ or 35.1 ± 0.4 pptv)
22 and oceanic emissions ($6 \pm 1\%$ or 5.62 ± 0.06 pptv). For the “non-meso” scenario, the
23 contributions of biomass burning ($46 \pm 2\%$ or 34.2 ± 0.7 pptv) and secondary
24 formation ($44 \pm 2\%$ or 32.9 ± 0.7 pptv) were comparable, and the oceanic emissions
25 contributed $10 \pm 1\%$ or 7.0 ± 0.07 pptv to the total alkyl nitrates. The higher
26 contribution of secondary formation in the “meso” scenario at TW was mainly
27 associated with higher degree of photochemical reactions. Indeed, the PBM-MCM
28 model simulation indicated that the average concentration of HO_x (HO_x = OH + HO₂)
29 during daytime hours (0700-1800 LT) in the “meso” scenario was $(2.5 \pm 0.7) \times 10^7$
30 molecule/cm³, about twice that of the “non-meso” scenario.

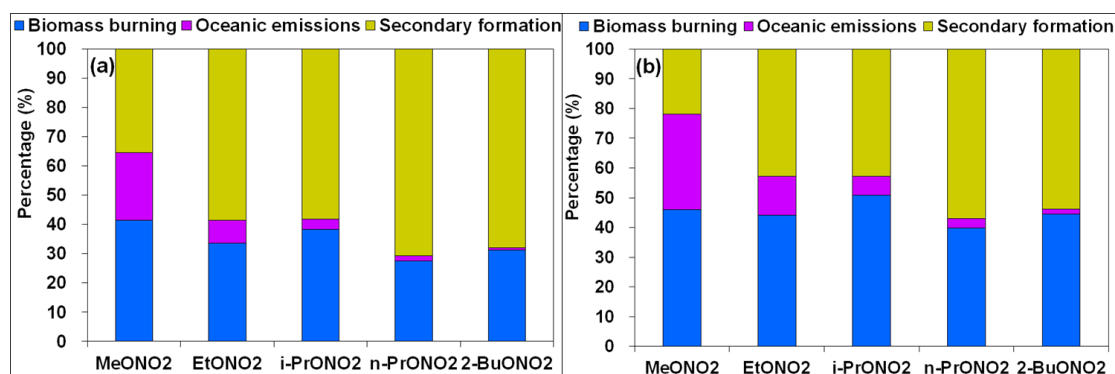


Figure 8. Source contributions to individual alkyl nitrates in (a) “meso” and (b) “non-meso” scenarios at TW (in percentage).

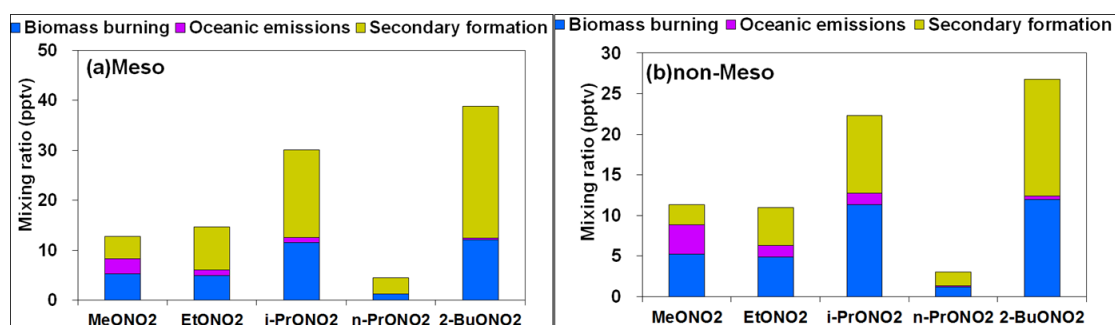
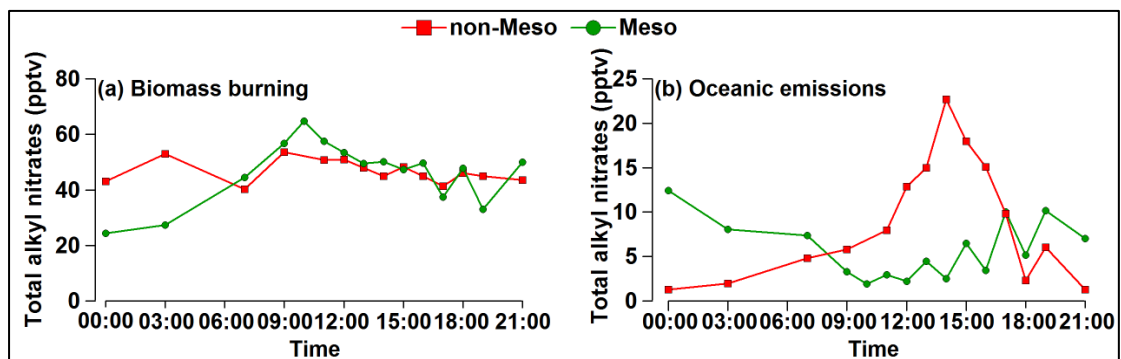


Figure 9. Source contributions to individual alkyl nitrates in (a) “meso” and (b) “non-meso” scenarios at TW (in summed mixing ratio).

In addition, although the percentage contribution of biomass burning was higher in the “non-meso” scenario, the absolute mixing ratios of biomass burning were comparable in the two scenarios. Figure 10 shows the diurnal patterns of Σ RONO₂ from biomass burning and oceanic emissions in “meso” and “non-meso” scenarios at TW. The contribution of biomass burning in the “meso” scenario was likely attributable to local emissions, including the cooking/heating activities in the small villages nearby and the frequent barbecue activities at the base of the mountain (Guo et al., 2013a, b), as well as the forest fires observed in the mountainous areas (AFCD, 2015). The regular cooking/heating activities from 0700 to 1400 LT in many dim sum restaurants in the village likely resulted in the increased levels of biomass burning in the morning until noon. In contrast, the diurnal pattern in “non-meso” scenario was weak and the maximum values were not statistically different from the minimum values. The difference of the average mixing ratio of Σ RONO₂ between daytime and nighttime hours was only 1 pptv for biomass burning. The weak diurnal variations in

1 the “non-meso” scenario suggests that the contribution of fresh biomass burning
 2 emissions was insignificant, revealing the influence of regional transport from the
 3 PRD region. This speculation was confirmed by the analysis of 12-h backward
 4 trajectories, which showed that air masses in the “non-meso” scenario were mainly
 5 from the inland PRD region (not shown). It is noteworthy that although air masses
 6 were more aged in the “non-meso” scenario, the levels of alkyl nitrates were
 7 comparable to those in the “meso” scenario, highlighting the strong emissions of
 8 biomass burning in the PRD region (Yuan et al., 2010).

9 For the oceanic emissions, a minimum mixing ratio during daytime hours was
 10 found for ΣRONO_2 in the “meso” scenario, while a broad peak was present during
 11 daytime hours in the “non-meso” scenario. The daytime minimum mixing ratio in the
 12 “meso” scenario at TW was related to uplifted valley breezes that brought alkyl
 13 nitrates away from TW to TMS, while the higher nighttime values were probably
 14 owing to marine emissions and aged continental plumes which were re-circulated
 15 from the South China Sea to the coastal urban site at night. In contrast, the broad
 16 daytime peak in the “non-meso” scenario was likely associated with higher daytime
 17 temperature and solar radiation, leading to higher oceanic emissions that were
 18 transported from eastern China and southern China coastal regions to the TW site.



19
 20 Figure 10. Diurnal patterns of (a) biomass burning and (b) oceanic emissions for
 21 “meso” and “non-meso” scenarios at TW.
 22

23 Moreover, the contributions of oceanic emissions to C_1 - C_2 alkyl nitrates were
 24 higher than C_3 - C_4 alkyl nitrates, with average percentages of 23% and 32% for the
 25 “meso” and “non-meso” scenarios (Figures 8 and 9), suggesting the importance of
 26 oceanic emissions to C_1 - C_2 alkyl nitrates, consistent with the results of previous work

1 (Simpson et al., 2003). The C₃-C₄ alkyl nitrates were dominated by the secondary
2 formation in the “meso” scenario (58-71%), while the contributions of biomass
3 burning and secondary formation to C₃-C₄ alkyl nitrates were comparable in the
4 “non-meso” scenario.

5 6 **3.2.3. Contributions of mesoscale circulation, in-situ formation and regional** 7 **transport to alkyl nitrates at TMS**

8 Valley breezes transported freshly-emitted parent hydrocarbons and alkyl nitrates
9 from the urban areas at the base of the mountain (TW) to the mountain summit (TMS)
10 during daytime hours, redistributing the ambient levels of alkyl nitrates at TMS (Guo
11 et al., 2013a; Lam et al., 2013). Except for MeONO₂, which had comparable levels in
12 both “meso” and “non-meso” scenarios, the mixing ratios of daytime C₂-C₄ alkyl
13 nitrates were all higher in “meso” scenario than those in “non-meso” scenario ($p <$
14 0.05), with the average values of 14.21 ± 0.79 , 28.73 ± 1.70 , 4.67 ± 0.29 and 40.21 ± 2.79
15 pptv for EtONO₂, *i*-PrONO₂, *n*-PrONO₂ and 2-BuONO₂, respectively. To quantify the
16 influence of mesoscale circulation on the mixing ratios of alkyl nitrates at TMS, a
17 moving box model coupled with master chemical mechanism (Mbox) was applied to
18 the data collected on the days influenced by mesoscale circulation (*i.e.*, “meso”
19 scenario) (Guo et al., 2013a). The model was developed based on an idealized
20 trajectory movement between TMS and TW sites, with air pollutants transported from
21 TW to TMS through the valley breeze during daytime hours (0800-1700 LT) when
22 photochemical formation of alkyl nitrates was occurring, contributing to their ambient
23 levels at TMS. As such, the model was only constrained with the observed daytime
24 data at TW. On the other hand, the night-time downslope flow occurred because of the
25 mountain breeze after sunset until the next morning, and TMS was set as the center of
26 the box model, which was constrained by the data collected at TMS only for that
27 period (Lam et al., 2013).

28 Table 3 presents the average concentrations of C₁-C₄ alkyl nitrates simulated by
29 the Mbox model at TMS, *i.e.*, the values under the “meso” scenario. It should be
30 noted that the comparison was only made for daytime alkyl nitrates (0800-1700LT),
31 when the valley breeze occurred. The average mixing ratios of MeONO₂, EtONO₂,

1 1-PrONO₂, 2-PrONO₂ and 2-ButONO₂ at daytime hours estimated using the Mbox
2 model were 9.97 ± 0.85 , 7.38 ± 0.44 , 3.08 ± 0.16 , 18.7 ± 0.77 and 34.7 ± 3.14 pptv,
3 respectively, accounting for 86%, 52%, 66%, 65% and 86% of the observed values at
4 TMS during the same period, respectively. These results demonstrate that when there
5 was mesoscale circulation, the alkyl nitrate levels at TMS were dominated by the
6 photo-oxidation of their parent hydrocarbons that originated from the urban site TW.
7 Although the mixing ratios of the parent hydrocarbons were lower at TMS, this is still
8 one possible explanation leading to the similar levels of alkyl nitrates measured at the
9 two sites.

10 For the “non-meso” scenario, the simulated levels of in-situ formation of
11 MeONO₂, EtONO₂, 1-PrONO₂, 2-PrONO₂ and 2-BuONO₂ at TMS were 3.61 ± 0.48 ,
12 2.18 ± 0.29 , 1.03 ± 0.13 , 3.68 ± 0.45 and 10.9 ± 1.31 pptv, respectively, accounting for
13 18-42% of the observed C₁-C₄ alkyl nitrates, indicating that other sources rather than
14 local photochemical formation made significant contributions to ambient levels of
15 alkyl nitrates. As stated earlier, TMS was a mountain site with sparse anthropogenic
16 emissions nearby. However, the prevailing synoptic northerly winds in “non-meso”
17 scenario suggested possible regional sources of alkyl nitrates from inland PRD region
18 to the mountain site. The impact of regional transport on the variations of air
19 pollutants at TMS for the days without mesoscale circulation, especially when the
20 prevailing winds were from the north with high speeds, was corroborated in Guo et al.
21 (2013a). By excluding the locally-formed alkyl nitrates from their overall levels, the
22 contribution of regional sources to alkyl nitrates was determined for TMS. The
23 regional source contributions to MeONO₂, EtONO₂, 1-PrONO₂, 2-PrONO₂ and
24 2-BuONO₂ were 7.07 ± 0.50 , 8.44 ± 0.62 , 2.11 ± 0.22 , 16.86 ± 1.17 , and 15.15 ± 1.49
25 pptv, respectively, accounting for 58-82% of the alkyl nitrates measured at TMS. It is
26 noteworthy that the regional alkyl nitrates included influences from all source
27 categories (photochemical formation, biomass burning and oceanic emissions) for the
28 inland PRD region.

29
30

1 Table 3. Mixing ratios of C₁-C₄ alkyl nitrates influenced by mesoscale circulation
 2 (“Meso”), in-situ formation and regional transport at TMS (unit: pptv).

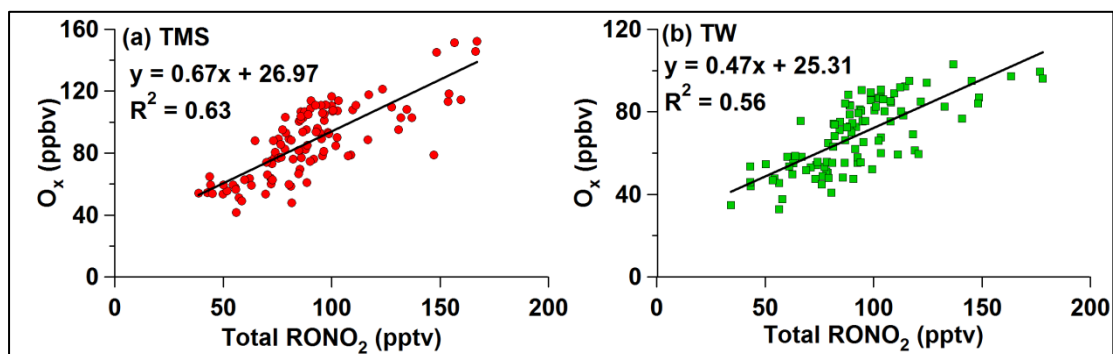
Scenario	MeONO ₂	EtONO ₂	1-PrONO ₂	2-PrONO ₂	2-BuONO ₂
“Meso”	9.97 ± 0.85	7.38 ± 0.44	3.08 ± 0.16	18.7 ± 0.77	34.7 ± 3.14
In-situ formation	3.61 ± 0.48	2.18 ± 0.29	1.03 ± 0.13	3.68 ± 0.45	10.9 ± 1.31
Regional transport	7.07 ± 0.50	8.44 ± 0.62	2.11 ± 0.22	16.86 ± 1.17	15.15 ± 1.49

3

4 **3.3. Relationship of alkyl nitrates with O₃**

5 Alkyl nitrates are mainly formed through the reaction of peroxy radical (RO₂)
 6 and NO. However, NO can be oxidized by RO₂ to form NO₂, which results in
 7 tropospheric O₃ formation through NO₂ photolysis. Hence, investigating the
 8 relationship between alkyl nitrates and O₃ is useful for evaluating the influence of
 9 alkyl nitrates on O₃ formation (Simpson et al., 2006). Since photochemical formation
 10 of O₃ and alkyl nitrates occurs during daytime hours, the relationship between O₃ and
 11 alkyl nitrates is usually evaluated using the observed daytime data (*i.e.*, 0900-1600
 12 LT). In this study, the “oxidant” O_x (O₃ + NO₂) was considered to be a better
 13 representation of O₃ levels as it takes into account the effect of O₃ titration by NO.
 14 Figure 11 shows the correlation between O_x and the total alkyl nitrates (ΣRONO₂) at
 15 daytime hours. Good correlations were found at TMS (R² = 0.63) and TW (R² = 0.56)
 16 with the slopes of 0.67 and 0.47 ppbv/pptv, respectively, suggesting that when 1 pptv
 17 of total alkyl nitrates were formed from the reaction of RO₂ and NO, 0.67 and 0.47
 18 ppbv of O_x could be simultaneously produced at TMS and TW, respectively. The
 19 relatively higher slope at TMS than at TW was owing to higher concentrations of HO_x
 20 radicals and higher photochemical reactivity of VOCs at TMS (Lyu et al., 2016).
 21 Additionally, as the formation of alkyl nitrates consumes NO, this process results in a
 22 negative contribution to O₃ formation. To quantify the negative influence on O₃, the
 23 PBM-MCM model was applied to the whole data collected at TMS and TW,
 24 respectively (Lyu et al., 2016). The formation of alkyl nitrates made negative
 25 contributions to the O₃ production, with the average reduction of 64.6 (TW: 24.9),
 26 37.4 (11.0), 18.9 (2.6), 39.6 (11.1), and 115.1 (40.6) pptv of O₃ for the formation of

1 MeONO₂, EtONO₂, 1-PrONO₂, 2-PrONO₂ and 2-BuONO₂ at TMS, respectively.
2 Furthermore, moderate to good correlation was found between the simulated O₃
3 reduction and the photochemically formed alkyl nitrates at TMS (R² = 0.42) and TW
4 (R² = 0.72), with the average O₃ reduction rate of 4.1 and 4.7 pptv/pptv, respectively.
5 Namely, O₃ was reduced by 4.1 and 4.7 pptv if 1 pptv of alkyl nitrates were formed at
6 TMS and TW, respectively.



7
8 Figure 11. Correlation between O_x (O₃ + NO₂) and total alkyl nitrates at (a) TMS and
9 (b) TW.

10
11 Moreover, because secondary alkyl nitrates are formed through two main
12 reaction pathways, “RO₂ + NO” and “RO + NO₂”, it is of interest to investigate the
13 relative contribution of the above pathways to the formation of alkyl nitrates. Two
14 scenarios for model simulations were run and compared. The first scenario was the
15 base case in which the model was run with all reaction pathways opened, while the
16 second scenario was the constrained case in which the pathway of RO₂ + NO →
17 RONO₂ was shut down. It was found that the reaction of “RO₂ + NO” was the
18 prominent pathway for the secondary formation of alkyl nitrates at the two sites. The
19 contributions of CH₃O₂ + NO to MeONO₂ accounted for about 72% and 50% of the
20 secondarily formed MeONO₂, while the contributions of RO₂ + NO were 97-99 and
21 95-99% of the secondarily formed C₂-C₄ alkyl nitrates at TMS and TW, respectively.
22 These results are similar to the findings obtained at Tai O, Hong Kong (Lyu et al.,
23 2015). The lower contributions of RO₂ + NO to MeONO₂ at the two sites were related
24 to the higher levels of CH₃O from the oxidation of CH₄ and the decomposition of
25 larger RO₂ radicals.

26

1 **4. Conclusions**

2 Intensive field measurements of alkyl nitrates and their parent hydrocarbons
3 were conducted concurrently at a mountain site (TMS) and an urban site (TW) at the
4 base of the same mountain in Hong Kong from September to November 2010. The
5 levels of MeONO₂, EtONO₂ and 2-PrONO₂ were slightly higher at TW than at TMS
6 ($p < 0.05$), while the average mixing ratios of 1-PrONO₂ and 2-BuONO₂ were
7 comparable at the two sites ($p > 0.05$). However, the levels of the parent hydrocarbons
8 of alkyl nitrates were lower at TMS, implying the complexity of sources of alkyl
9 nitrates. Receptor model and photochemical box model simulations found that
10 mesoscale circulation and regional transport had a significant impact on the levels of
11 alkyl nitrates at the two sites. At TW, secondary formation was the dominant
12 contributor to alkyl nitrates when there was mesoscale circulation, while the
13 contributions of secondary formation and biomass burning were comparable under the
14 influence of regional transport. At TMS, photo-oxidation of the parent hydrocarbons
15 from TW contributed 52-85% to the ambient levels of alkyl nitrates on the days with
16 mesoscale circulations between the two sites. On the other hand, alkyl nitrates from
17 the inland PRD region were responsible for 58-82% of the observed values at TMS on
18 the days with regional influence. The photo-oxidation of parent hydrocarbons from
19 TW and regional transport resulted in similar values of alkyl nitrates observed at the
20 two sites. With regard to the secondarily formed alkyl nitrates, the reaction of RO₂
21 and NO was the prominent pathway at both sites. Moreover, the formation of alkyl
22 nitrates made negative contributions to the O₃ formation, with a reduction rate of 4.1
23 and 4.7 pptv O₃ per pptv alkyl nitrates at TMS and TW, respectively. The findings of
24 this study will aid in understanding the source contributions and photochemical
25 formation pathways of alkyl nitrates in Hong Kong's mountainous areas.

26 27 **Acknowledgements**

28 This project was supported by the Research Grants Council of the Hong Kong Special
29 Administrative Region via grants PolyU5154/13E, PolyU152052/14E and
30 CRF/C5022-14G. This study was partly supported by the internal grants of the Hong

1 Kong Polytechnic University (4-BCAV and 1-ZVCX), and the National Natural
2 Science Foundation of China (No. 41405112 and 41275122). The challenging but
3 ultimately very helpful comments of the anonymous reviewers are greatly
4 appreciated.

5 **References**

- 6 AFCD (Agriculture, Fisheries and Conservation Department), 2008. Available at website:
7 <http://www.afcd.gov.hk/>.
- 8 AFCD (Agriculture, Fisheries and Conservation Department), useful statistics, Last Review Date
9 02 June 2015. Available at website: [http://www.afcd.gov.hk/english/country/cou_lea/
10 cou_lea_use/cou_lea_use.html](http://www.afcd.gov.hk/english/country/cou_lea/cou_lea_use/cou_lea_use.html).
- 11 Archibald, A.T., Khan, M.A.H., Watson, L.A., Utembe, S.R., Shallcross, D.E., Clemittshaw, K.C.,
12 Jenkin, M.E., 2007. Comment on 'Long-term atmospheric measurements of C₁-C₅ alkyl
13 nitrates in the Pearl River Delta region of southeast China' by Simpson et al. *Atmospheric
14 Environment* 41, 7369-7370.
- 15 Arey, J., Aschmann, S.M., Kwok, E.S.C., Atkinson, R., 2001. Alkyl nitrate, hydroxyl nitrate, and
16 hydroxycarbonyl formation from the NO_x-air photooxidations of C₅-C₈ n-alkanes. *Journal
17 of Physical Chemistry* 105, 1020-1027.
- 18 Atkinson, R., Baulch, D.L., Cox, R.A., Crowley, J.N., Hampson, R.F., Hynes, R.G., Jenkin, M.E.,
19 Rossi, M.J., Troe, J., Subcommittee, I., 2006. Evaluated kinetic and photochemical data for
20 atmospheric chemistry: volume II – gas phase reactions of organic species. *Atmospheric
21 Chemistry and Physics* 6, 3625-4055.
- 22 Barletta, B., Meinardi, S., Simpson, I.J., Atlas, E.L., Beyersdorf, A.J., Baker, A.K., Blake, N.J.,
23 Yang, M., Midyett, J.R., Novak, B.J., Mckeachie, R.J., Fuelberg, H.E., Sachse, G.W., Avery,
24 M.A., Campos, T., Weinheimer, A.J., Rowland, F.S., Blake, D.R., 2009. Characterization of
25 volatile organic compounds (VOCs) in Asian and north American pollution plumes during
26 INTEX-B: identification of specific Chinese air mass tracers. *Atmospheric Chemistry and
27 Physics* 9, 5371-5388.
- 28 Barletta, B., Meinardi, S., Simpson, I.J., Khwaja, H.A., Blake, D.R., Rowland, F.S., 2002. Mixing
29 ratios of volatile organic compounds (VOCs) in the atmosphere of Karachi, Pakistan.
30 *Atmospheric Environment* 36, 3429-3443.
- 31 Bertman, S.B., Roberts, J.M., Parrish, D.D., Buhr, M.P., Goldan, P.D., Kuster, W.C., Fehsenfeld,
32 F.C., Montzka, S.A., Westberg, H., 1995. Evolution of alkyl nitrates with air mass age.
33 *Journal of Geophysical Research* 100, 22805-22813.
- 34 Blake, N.J., D. R. Blake, A. L. Swanson, E. Atlas, F. Flocke, and F. S. Rowland, 2003. Latitudinal,
35 vertical, and seasonal variations of C₁-C₄ alkyl nitrates in the troposphere over the Pacific
36 Ocean during PEM-Tropics A and B: Oceanic and continental sources, *Journal of
37 Geophysical Research* 108(D2), 8242, doi:10.1029/2001JD001444, 2003.

1 Clemitshaw, K.C., Williams, J., Rattigan, O.V., Shallcross, D.E., Law, K.S., Cox, R.A., 1997.
2 Gas-phase ultraviolet absorption cross-sections and atmospheric lifetimes of several C₂–C₅
3 alkyl nitrates. *Journal of Photochemistry and Photobiology A: Chemistry* 102, 117–126.

4 Gao, J., Wang, T., Ding, A.J., Liu, C.B., 2005. Observation study of ozone and carbon monoxide
5 at the summit of mount Tai (1534 m a.s.l.) in central-eastern China. *Atmospheric*
6 *Environment* 39, 4779-4791.

7 Guo, H., Jiang, F., Cheng, H.R., Simpson, I.J., Wang, X.M., Ding, A.J., Wang, T.J., Saunders, S.M.,
8 Wang, T., Lam, S.H.M., Blake, D.R., Zhang, Y.L., Xie, M., 2009. Concurrent observations of
9 air pollutants at two sites in the Pearl River Delta and the implication of regional transport.
10 *Atmospheric Chemistry and Physics* 9, 7343-7360.

11 Guo, H., Cheng, H.R., Ling, Z.H., Louie, P.K.K., Ayoko, G.A., 2011. Which emission sources are
12 responsible for the volatile organic compounds in the atmosphere of Pearl River Delta?
13 *Journal of Hazardous Materials* 188, 116-124.

14 Guo, H., Ling, Z.H., Cheung, K., Jiang, F., Wang, D.W., Simpson, I.J., Barletta, B., Meinardi, S.,
15 Wang, T.J., Wang, X.M., Saunders, S.M., Blake, D.R., 2013a. Characterization of
16 photochemical pollution at different elevations in mountainous areas in Hong Kong.
17 *Atmospheric Chemistry and Physics* 13, 3881-3898.

18 Guo, H., Ling, Z.H., Cheung, K., Wang, D.W., Simpson, I.J., Blake, D.R., 2013b. Acetone in the
19 atmosphere of Hong Kong: Abundance, sources and photochemical precursors. *Atmospheric*
20 *Environment* 65, 80-88.

21 Guo, H., Ling, Z.H., Simpson, I.J., Blake, D.R., Wang, D.W., 2012. Observations of isoprene,
22 methacrolein (MAC) and methyl vinyl ketone (MVK) at a mountain site in Hong Kong.
23 *Journal of Geophysical Research* 117, doi:10.1029/2012JD017750.

24 HKCSD (Hong Kong Census and Statistics Department), 2010. Hong Kong Energy Statistics:
25 Annual Report. <http://www.censtatd.gov.hk>.

26 HKEPD (Hong Kong Protection Department), 2012. Air Quality in Hong Kong.
27 2011. <http://www.epd-asg.gov.hk/english/report/aqr.html>.

28 Jenkin, M. E., Saunders, S. M., Wagner, V., and Pilling, M. J., 1997. The tropospheric degradation
29 of volatile organic compounds: A protocol for mechanism development. *Atmospheric*
30 *Environment* 31, 81-107, 1997.

31 Jenkin, M. E., Saunders, S. M., Wagner, V., and Pilling, M. J., 2003. Protocol for the development
32 of the master chemical mechanism MCMv3 (Part B): Tropospheric degradation of aromatic
33 volatile organic compounds, *Atmospheric Chemistry and Physics* 3, 181-193, 2003.

34 Jenkin, M.E., Clemitshaw, C., 2000. Ozone and other secondary photochemical pollutants:
35 Chemical processes governing their formation in the planetary boundary layer. *Atmospheric*
36 *Environment* 34, 2499-2527.

37 Jiang, F., Guo, H., Wang, T.J., Cheng, H.R., Wang, X.M., Simpson, I.J., Ding, A.J., Saunders, S.M.,
38 Lam, S.H.M., Blake, D.R., 2010. An O₃ episode in the Pearl River Delta: field observation
39 and model simulation. *Journal of Geophysical Research* 115, doi:/10.1029/2009JD013583.

- 1 Kwok, E.S.C. and Atkinson, R., 1995. Estimation of hydroxyl radical reaction-rate constants for
2 gas-phase organic-compounds using a structure-reactivity relationship-an update.
3 *Atmospheric Environment* 29, 1685-1695.
- 4 Lam, S.H.M., Saunders, S.M., Guo, H., Ling, Z.H., Jiang, F., Wang, X.M., Wang, T.J., 2013.
5 Modelling VOC source impacts on high ozone episode days observed at a mountain summit
6 in Hong Kong under the influence of mountain-valley breezes. *Atmospheric Environment* 81,
7 166-176.
- 8 Lau, A. K.H., Yuan, Z.B., Yu, J.Z., Louie, P.K.K., 2010. Source apportionment of ambient volatile
9 organic compounds in Hong Kong. *Science of the Total Environment* 408, 4138-4149.
- 10 Ling, Z.H. and Guo, H., 2014. Contribution of VOC sources to photochemical ozone formation
11 and its control policy implication in Hong Kong. *Environmental Science and Policy* 38,
12 180-191.
- 13 Ling, Z.H., Guo, H., Cheng, H.R., Yu, Y.F., 2011. Sources of ambient volatile organic compounds
14 and their contributions to photochemical ozone formation at a site in the Pearl River Delta,
15 southern China. *Environmental Pollution* 159, 2310-2319.
- 16 Ling, Z.H., Guo, H., Lam, S.H.M., Saunders, S.M., Wang, T., 2014. Atmospheric photochemical
17 reactivity and ozone production at two sites in Hong Kong: Application of a Master Chemical
18 Mechanism-photochemical box model. *Journal of Geophysical Research* 119,
19 doi:10.1002/2014JD021794.
- 20 Lyu, X.P., Ling, Z.H., Guo, H., Zeng, L.W., Wang, N., 2016. Impact of alkyl nitrate chemistry on
21 photochemical reactivity and O₃ production in Hong Kong. In preparation.
- 22 Lyu, X.P., Ling, Z.H., Guo, H., Saunders, S.M., Lam, S.H.M., Wang, N., Wang, Y., Liu, M., Wang,
23 T., 2015. Re-examination of C₁-C₅ alkyl nitrates in Hong Kong using an observation-based
24 model. *Atmospheric Environment* 120, 28-37.
- 25 Marandino, C.A., Tegtmeier, S., Krüger, K., Zindler, C., Atlas, E.L., Moore, F., Bange, H.W., 2013.
26 Dimethylsulphide (DMS) emissions from the western Pacific Ocean: a potential marine
27 source for stratospheric sulphur? *Atmospheric Chemistry and Physics* 13, 8427-8437.
- 28 Paatero, P., 2000. User's guide for Positive Matrix Factorization Programs PMF2 and PMF3, part
29 1: Tutorial. Prepared by University of Helsinki, Finland (February).
- 30 Pinho, P.G., Lemos, L.T., Pio, C.A., Evtugina, M.G., Nunes, T.V., Jenkin, M.E., 2009. Detailed
31 chemical analysis of regional-scale air pollution in western Portugal using an adapted version
32 of MCM v3.1. *Science of the Total Environment* 407, 2024-2038.
- 33 Reeves, C.E., Slemr, J., Oram, D.E., Worton, D., Penkett, S.A., Stewart, D.J., Purvis, R., Watson,
34 N., Hopkins, J., Lewis, A., Methven, J., Blake, D.R., Atlas, E., 2007. Alkyl nitrates in outflow
35 from North America over the North Atlantic during intercontinental transport of ozone and
36 precursors 2004. *Journal of Geophysical Research* 112, D10S037, doi:
37 10.1029/2006JD007567.
- 38 Roberts, J.M., Bertman, S.B., Parrish, D.D., Fehsenfeld, F.C., Johnson, B.T., Niki, H., 1998.
39 Measurements of alkyl nitrates at Chebogue Point Nova Scotia during the 1993 North

1 Atlantic Regional Experiment (NARE) intensive. *Journal of Geophysical Research* 103 (D11),
2 13569-13580.

3 Russo, R.S., Zhou, Y., Haase, K.B., Wingenter, O.W., Frinak, E.K., Mao, H., Talbot, R.W., Sive,
4 B.C., 2010. Temporal variability, sources and sinks of C₁-C₅ alkyl nitrates in coastal New
5 England. *Atmospheric Chemistry and Physics* 10, 1865-1883.

6 Saunders, S. M., Jenkin, M. E., Derwent, R. G., and Pilling, M. J., 2003. Protocol for the
7 development of the master chemical mechanism MCMv3 (Part A): Tropospheric degradation
8 of non-aromatic volatile organic compounds. *Atmospheric Chemistry and Physics* 3,
9 161-180.

10 Seinfeld, J.H. and Pandis, S.N., 2006. *Atmospheric Chemistry and Physics: from air pollution to*
11 *climate change*, 2nd edition. Wiley Publisher, New Jersey, USA.

12 Simpson, I.J., Akagi, S.K., Barletta, B., Blake, N.J., Choi, Y., Diskin, G.S., Fried, A., Fuelberg,
13 H.E., Meinardi, S., Rowland, F.S., Vay, S.A., Weinheimer, A.J., Wennberg, P.O., Wiebring, P.,
14 Wisthaler, A., Yang, M., Yokelson, R.J., Blake, D.R., 2011. Boreal forest fire emissions in
15 fresh Canadian smoke plumes: C₁-C₁₀ volatile organic compounds (VOCs), CO₂, CO, NO₂,
16 NO, HCN and CH₃CN. *Atmospheric Chemistry and Physics* 11, 6445–6463.

17 Simpson, I.J., Blake, N.J., Barletta, B., Diskin, G.S., Fuelberg, H.E., Gorham, K., Huey, L.G.,
18 Meinardi, S., Rowland, F.S., Vay, S.A., Weinheimer, A.J., Yang, M., Blake, D.R., 2010.
19 Characterization of trace gases measured over Alberta oil sands mining operations: 76
20 speciated C₂-C₁₀ volatile organic compounds (VOCs), CO₂, CH₄, CO, NO, NO₂, NO_y, O₃ and
21 SO₂. *Atmospheric Chemistry and Physics* 10, 11931-11954.

22 Simpson, I.J., Blake, N.J., Blake, D.R., Atlas, E., Flocke, F., Crawford, J.H., Fuelberg, H.E., Kiley,
23 C.M., Meinardi, S., Rowland, F.S., 2003. Photochemical production and evolution of selected
24 C₂-C₅ alkyl nitrates in tropospheric air influenced by Asia outflow. *Journal of Geophysical*
25 *Research* 108, D20, doi:10.1029/2002JD002830.

26 Simpson, I.J., Meinardi, S., Blake, D.R., Blake, N.J., 2002. A biomass burning source of C₁-C₄
27 alkyl nitrates. *Geophysical Research Letters* 29 (24), 2168, doi: 10.1029/2002GL016290.

28 Simpson, I.J., Wang, T., Guo, H., Kwok, Y.H., Flocke, F., Atlas, E., Meinardi, S., Rowland, F.S.,
29 Blake, D.R., 2006. Long-term atmospheric measurements of C₁-C₅ alkyl nitrates in the Pearl
30 River Delta region of southeast China. *Atmospheric Environment* 40, 1619-1632.

31 Sommariva, R., Trainer, M., de Gouw, J.A., Roberts, J.M., Warneke, C., Atlas, E., Flocke, F.,
32 Goldan, P.D., Kuster, W.C., Swanson, A.L., Fehsenfeld, F.C., 2008. A study of organic
33 nitrates formation in an urban plume using a Master Chemical Mechanism. *Atmospheric*
34 *Environment* 42, 5771-5786.

35 Talukdar, R.K., Burkholder, J.B., Hunter, M., Gilles, M.K., Roberts, J.M., Ravishankara, A.R.,
36 1997. Atmospheric fate of several alkyl nitrates Part 2 UV absorption cross-sections and
37 photodissociation quantum yields. *Journal of the Chemical Society, Faraday Transactions* 93,
38 2797–2805.

39 Wang, M., Shao, M., Chen, W.T., Lu, S.H., Wang, C., Huang, D.K., Yuan, B., Zeng, L.M., Zhao,

1 Y., 2013. Measurements of C₁-C₄ alkyl nitrates and their relationships with carbonyl
2 compounds and O₃ in Chinese cities. *Atmospheric Environment* 81, 389-398.

3 Wang, T., Poon, C.N., Kwok, Y.H., Li, Y.S., 2003. Characterizing the temporal variability and
4 emission patterns of pollution plumes in the Pearl River Delta of China. *Atmospheric*
5 *Environment* 37, 3539-3550.

6 Wang, T., Wong, H.L.A., Tang, J., Ding, A., Wu, W.S., Zhang, X.C., 2006. On the origin of surface
7 ozone and reactive nitrogen observed at a remote site in the northeastern Qinghai-Tibetan
8 Plateau, western China. *Journal of Geophysical Research* 111, D08303, doi:
9 10.1029/2005JD006527.

10 Worton, D.R., Reeves, C.E., Penkett, S.A., Sturges, W.T., Slemr, J., Oram, D.E., Bandy, B.J.,
11 Bloss, W.J., Carslaw, N., Davey, J., Emmerson, K.M., Gravestock, T.J., Hamilton, J.F., Heard,
12 D.E., Hopkins, J.R., Hulse, A., Ingram, T., Jacob, M.J., Lee, J.D., Leigh, R.J., Lewis, A.C.,
13 Monks, P.S., Smith, S.C., 2010. Alkyl nitrate photochemistry during the tropospheric organic
14 chemistry experiment. *Atmospheric Environment* 44, 773-785.

15 Wu, Z.Y., Wang, X.M., Chen, F., Turnipseed, A.A., Guenther, A., Niyogi, D., Charusombat, U.,
16 Xia, B.C., Munger, J.W., Alapty, K., 2011. Evaluating the calculated dry deposition velocities
17 of reactive nitrogen oxides and ozone from two community models over a temperate
18 deciduous forest. *Atmospheric Environment* 45, 2633-2674.

19 Yuan, B., Liu, Y., Shao, M., Lu, S.H., Streets, D.G., 2010. Biomass burning contributions to
20 ambient VOCs species at a receptor site in the Pearl River Delta (PRD), China.
21 *Environmental Science and Technology* 44, 4577-4582.

22

23

24